#### **RESEARCH PAPER**



# Numerical and Experimental Study of Trajectory for Free-Falling Jets

Ali Taheri Aghdam<sup>1</sup> · Ali Hosseinzadeh Dalir<sup>1</sup> · Farzin Salmasi<sup>1</sup> · Akram Abbaspour<sup>1</sup> · John Abraham<sup>2</sup>

Received: 27 June 2022 / Accepted: 10 January 2023 © The Author(s), under exclusive licence to Shiraz University 2023

#### **Abstract**

The water flow over a dam spillway has a lot of energy, and if this energy is not dissipated, the flowing water can cause damage to the dam and downstream structures. One way to dissipate this extra energy is to expel water jets into a plunging pool. In the present study, the trajectories of free-falling jets are investigated both numerically and experimentally. Ansys Fluent software is used for numerical simulation, and laboratory work is carried out in the hydraulic laboratory of University of Tabriz, Iran. The results showed that a free-falling jet in a laboratory experiment has a shorter trajectory than its calculated value using projectile equations and simulations using Ansys Fluent software; this difference is because of air resistance. By reducing the outlet cross section of the free-falling jet and increasing the head passing through the dam spillway, the free-falling jet reaches the ground at a greater distance from the dam body. Since none of the equations presented for calculating the trajectory of jets have been obtained using laboratory results and have not considered air resistance, they over estimate by 21%, the trajectory jet. In the present study, equations are provided to calculate the trajectory of a free-falling jet including air resistance. The simulation results also showed that the velocity experiences a 247% increase compared to the velocity at the end of the dam overflow, when hits the ground. This increase in velocity requires more attention in the design of stilling basins at the end of dams.

**Keywords** Ansys Fluent · Air resistance · Free jet · Jet trajectory · Projectile equation

### 1 Introduction

Falling jets are one of the most important issues in hydraulic structures. Often these jets enter the plunge pool and lose their energy. The main mechanism of energy dissipation is the scattering of the jet into the air, followed by the entry of air into the jet, and finally the scattering and turbulence

☐ Farzin Salmasi Salmasi@tabrizu.ac.ir

Ali Taheri Aghdam alitaheriagdam@gmail.com

Ali Hosseinzadeh Dalir ahdalir@tabrizu.ac.ir

Akram Abbaspour akabbaspour@yahoo.com

John Abraham jpabraham@stthomas.edu

Published online: 23 January 2023

- Department of Water Engineering, Faculty of Agriculture, University of Tabriz, Tabriz, Iran
- School of Engineering, University of St. Thomas, Minnesota, 2115 Summit Avenue, St. Paul, MN 55105, USA

of the jet at the plunge pool (Salmasi and Abraham 2022). Falling water jets have a core that projects some distance and causes pressure increases on the bed and the wall of the pool. Along its trajectory, the jet core gradually shrinks because of the infiltration of air and from turbulence and eventually breaks apart (Salemnia and Fathi Moghadam 2019).

A falling jet with a velocity of  $v_0$  is launched from the dam crest. Considering the dam crest as the origin of the coordinates, the vertical position equation is taken from (USBR 1960):

$$y = x \tan \theta_0 - \frac{gx^2}{2v_0^2 \cos^2 \theta_0}$$
 (1)

In Eq. 1, x and y are the coordinates of the lower edge of the jet,  $v_0$  is the initial velocity of the jet,  $\theta_0$  is the initial angle of the jet from the horizon (zero if the jet is horizontal, positive if the jet issues upward, and negative if the jet is initially inclined downward), and g is the gravitational acceleration. When the jet begins horizontally (the initial angle of the jet from the horizon is zero), the equation is simplified as follows:



$$y = -\frac{gx^2}{2v_0^2} \tag{2}$$

These equations describe the motion of a projectile that is not affected by air resistance. In fact, the trajectory length calculated from these equations is greater than their true value due to air resistance. By placing  $h_v = v_0^2/2g$ , we can write:

$$y = x \tan \theta_0 - \frac{x^2}{4h_v \cos^2 \theta_0} \tag{3}$$

The trajectory of the upper surface of the jet can also be easily calculated by adding the thickness of the watery jet  $(t_0)$ , assuming that the velocity and orientation angle are the same at the lower edge of the jet. This means that the jet does not spread as it falls. That is, the cross section stays constant.

$$y = t_0 + x \tan \theta_0 - \frac{x^2}{4h_0 \cos^2 \theta_0} \tag{4}$$

In Eq. 4,  $t_0$  is the thickness of the watery jet (USBR 1976). It should be noted that although the above equation has used in the past, in reality, there is a shrinkage of the core of the jet along its path of motion; this fact limits the accuracy of Eq. 4. In the case of free fall of water from a dam, an equation similar to the equation of the jet trajectory is presented in the book Design of Small Dams (USBR 1960), which is used in the design of chutes in open canals, spillways, and other situations.

$$y = x \tan \theta_0 - \frac{x^2}{4K(d + h_v)\cos^2 \theta_0}$$
 (5)

where *d* is the flow depth. Equation 5 describes the trajectory of a free jet. This equation is modified by a factor of *K*. Research has shown that *K* values less than or equal to 1 (0.9 and 0.75 are usually recommended) provide the best jet trajectory (closer to reality). Equation 5 has also been used in the book Design of Gravity Dams (USBR 1976), the book Design of Arched Dams (USBR 1977) and in Annandale (2006) to predict the free jet trajectory of water from a dam.

Salmanzadeh et al. (2016) investigated the path of a free jet and provided equations for determining their kinetic distribution, regardless of the frictional force of the air. The following equation was provided to calculate the downward jet trajectory under pressure:

$$\frac{y}{h_0} = -0.162 \left(\frac{x}{h_0}\right)^2 - 0.415 \left(\frac{x}{h_0}\right) + 6.68 \tag{6}$$

In Eq. 6,  $h_0$  is the initial velocity head of the projectile.

A dimensionless equation was proposed by the US Army Corp Engineers (USACE 1964) to calculate the free-fall jet trajectory; Eq. 7 shows the resulting dimensionless equation.

$$\frac{x}{h_v} = \sin 2\theta_0 + 2\cos\theta_0 \sqrt{\sin^2\theta_0 + \frac{y}{h_v}} \tag{7}$$

Figure 1 provides a photograph of Karun III dam in Iran. This figure shows free-falling jets from dam spillways (left and central sides) as well as dam outlets. A large amount of air entrainment can be seen in flow that creates a two-phase air—water mixture.

Davis et al. (1999) proposed similar equations to calculate the upper nappe of water flow in a free-falling jet. They determined the initial velocity upstream of the edge of the free jet. Rouse (1943) referred to the Froude number in an upstream section and showed that the thickness of the vertical jet is almost constant. Wahl et al. (2008) examined and compared the trajectory of the free and pressurized falling jets. The results showed that when calculating the trajectory of a free jet, the initial velocity of the jet  $(V_0)$  or the initial velocity head  $(h_0)$  should always be used. The incomplete model that forms the basis of Eq. 5 should not be used to describe a free jet. Rouse (1936) conducted a laboratory study of free-fall flow from spillway. The results showed that the flow should pass from the critical depth on the crest and fall from the crest as a supercritical flow. Rouse (1936) showed that a flow with a depth of  $y_b = 0.715 y_c$  is thrown from the edge of the spillway crest. (In this relation,  $y_c$  is the critical depth on the spillway and  $y_b$  is the depth at the end of the spillway (spill site).) Henderson (1966) provides an excerpt of early work in this area, including the Delleur (1956) results on a spillway shown in Fig. 2.

In practice, to determine the depth and velocity at the point of flow on the spillway crest (depth and velocity are required to calculate the jet trajectory), the spillway equation  $Q = \text{CLH}^{1.5}$  is used. In which Q is the discharge, C is the discharge coefficient, L is the length of the spillway, and H is the depth of the water over the spillway crest. The critical depth  $(y_c)$  corresponding to the discharge is calculated from  $y_c = (q^2/g)^{1/3}$ , where q is the discharge per unit width of the crest (q = O/L).

The depth of water on the crest and at the location of the free-falling jet can be determined by using the equations given by Delleur (1956) or Rouse (1936), and the velocity of the flow at the crest and in the falling jet can be determined from the continuity equation. It should be noted that because the critical flow produces the minimum specific energy for a given flow rate, the specific energy at the edge of the spillway, where the flow is supercritical, will be greater than the specific energy in the critical section. This seems paradoxical, but since the pressure distribution at the edge of the spillway is not hydrostatic, the specific energy at the edge is





Fig. 1 Photograph of free-falling jets in Karun III dam in Iran

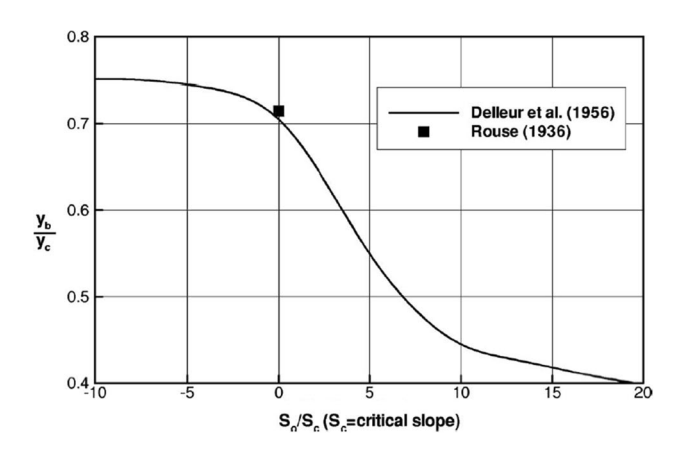


**Fig. 2** Ratio of water depth at the crest of a spillway to the critical depth for sloping and horizontal flows (Delleur 1956; Rouse 1936)

not obtained from the simple sum of  $y_b + v_b^2/2g$ . If the pressure distribution at the edge of the spillway was hydrostatic, the flow would return to the dam (the flow would move from more energy to less energy), but since the pressure distribution is not hydrostatic, the flow would fall from the spillway crest.

Salemnia et al. (2019) investigated the length of jet fracture and the parameters affecting it. The results showed that the velocity at the jet collision site is maximal and gradually decreases with distance from the collision site. The lowest speed and pressure as well as the lowest average fluctuations occur for the smallest jet diameters, which is related to a more substantial effect of air resistance.

Fluent software is one of the most powerful applied computational fluid dynamics (CFD) software and has been used to model fluid flow and heat transfer in complex geometries. This software makes it possible to change the mesh completely and analyze the flow with unstructured meshes for complex geometries (Ansys Fluent 2015). Among the research done with CFD, the following studies are stated.

Yildz et al. (2020) modeled a broad-crested weir both experimentally and numerically using Ansys Fluent software. An experimental and numerical simulation of flow over stepped spillways was carried out by Salmasi and Samadi (2018) using Fluent numerical model, and the investigation of the effect of upstream and downstream face slopes of a broad-crested weir was carried out by and Malekzadeh et al. (2022) using Fluent. Salmasi et al. (2022) investigated of wavelet flow conditions and flow rate coefficient



in rectangular broad-crested weir using the Ansys Fluent software. Despite this past research, it appears that no studies have been performed on the trajectory of free-falling jets.

In the present study, the characteristics of free-falling jets are investigated using physical models and CFD. In the above referenced literature and equations, the effect of air resistance has not been studied. In the present study, the effect of air resistance on the free-falling jet trajectory is investigated with a goal of improving the accuracy of jet trajectory predictions. To calculate the jet more accurately, air resistance is incorporated into the equations using coefficients. (In other words, the projectile motion equations are obtained in conditions where the effect of air resistance on the trajectory of the projectile is not taken into account. Therefore, the trajectory length calculated using the projectile equation (Eq. 3) is greater than its actual value due to the effect of air resistance. In the present study, Eq. 3 is modified to predict the trajectory of the projectile with less error.) The effect of the width of the outlet cross section of the free jet and the head passing through the dam to the jet is examined. A comparison is made between the equations presented by prior researchers, and the results of the

Table 1 Range of parameters used in study

Parameter	$V_0$ (m/s)	H <sub>ovetop</sub> (m)	D (m)	$X_{\text{max}}$ (m)
Maximum	1.55	0.22	0.12	1.15
Minimum	0.30	0.03	0.01	0
Average	0.85	0.15	0.06	0.65

laboratory and numerical studies of the present work will be used to calculate the trajectory of a free jet.

#### 2 Material and Methods

# 2.1 Geometric Specifications of the Physical Model

In the present study, experiments were performed in the hydraulic laboratory of the Faculty of Agriculture, Department of Water Engineering, University of Tabriz, Iran. A cubic tank with a length of 2 m, a width of 1.5 m, and a height of 1.2 m was used as a reservoir. A rectangular broadcrested weir was installed on this tank. At the downstream section, a flume was installed to transfer water to the main underground reservoir. In upstream section, a vertical cylindrical water tower was provided to supply the water needed to simulate the downstream free-falling jet. To provide the height required for the fall of the jet, the water tank was elevated 2 m. Parameters that affect the launch jet trajectory are listed in Table 1. Figure 3 shows a schematic diagram of the laboratory arrangement for measuring the trajectory of the jet.

In Fig. 3, x and y are the coordinates of the lower edge of the jet (in the present study, the coordinates origin is at the end of the broad-crested weir),  $X_{\text{max}}$  is the maximum range of the free-fall jets, and  $H_{\text{overtop}}$  is the water head over the spillway (overtopping head).

A camera was used to capture the data of the free-fall jet crash route. In this way, after establishing the flow of falling

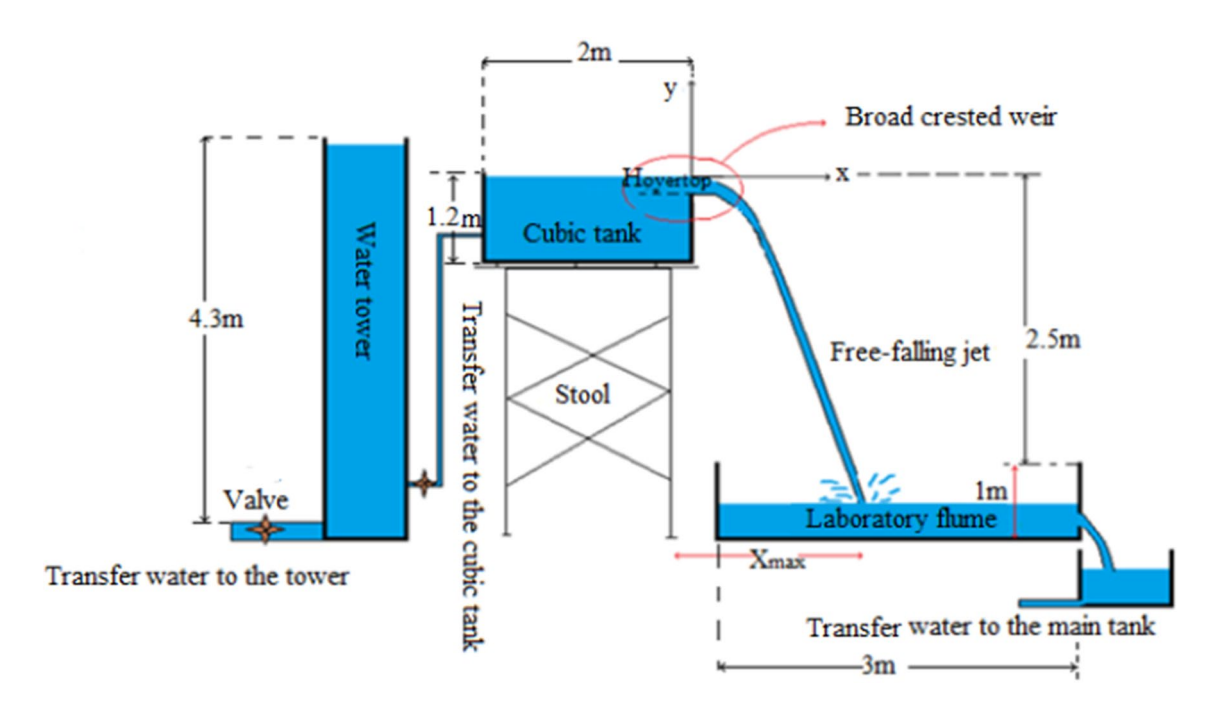


Fig. 3 Schematic of the free-falling jet laboratory facility



jet from the dam spillway (a rectangular broad-crested weir installed on the tank), photographs were taken of the trajectory of the falling jets. The x and y coordinates of the falling jets in these photographs were extracted using Plot-Digitizer software. The first four specific points on the image whose x and y values are known are entered into the software, and the coordinates are extracted. Thus, the coordinates of the trajectory of the falling jets are obtained. It should be noted that the discharge of the jet fall was measured by a volumetric method in all experiments. It is necessary to explain that in each of the experiments of the present study, the water level inside the tank is fixed. When the water level inside the tank is constant, the initial jet velocity ( $V_0$ ) and head passing through the structure (overtopping head) remain constant.

The software used in the present study was calibrated, and numerical simulations were performed for the models. Table 1 shows the range of parameters in the present study.

In the above table,  $H_{\rm overtop}$  is the water head over the spillway (overtopping head),  $V_0$  is the initial velocity of the jet,  $X_{\rm max}$  is the maximum range of the free-fall jets, and D is the width of the outlet of the free jet.

# 2.2 Numerical Simulation with Fluent software (Governing Equations)

The basis of the numerical method is the solution of flow equations including continuity and momentum equations, which are known as Navier–Stokes equations. For an incompressible flow with a constant viscosity, the equations are written in the form of Eqs. 8 and 9, respectively (Nourani et al. 2021).

$$\frac{\partial}{\partial X_i}(\overline{U_i}) = 0 \tag{8}$$

$$\frac{\partial U_i}{\partial t} + U_j \frac{\partial U_i}{\partial X_j} = \frac{1}{\rho} \frac{\partial}{\partial X_j} (-P \,\delta_{ij} - \rho \overline{U_i \, U_j}) \tag{9}$$

In the above equation,  $U_i$  and  $U_j$  are the components of the velocity vector in the spatial direction i and j, P is the pressure,  $\rho$  is the fluid density, and  $\delta_{i,j}$  is the Kronecker delta. (If i=j, its value is one, and otherwise its value is zero.) The first expression to the left of Eq. 9 is the transient term, and the second expression is the convective term. The first expression of the right of Eq. 9 is the pressure term, and the second expression is the Reynolds stress.

#### 2.3 Numerical Model

To incorporate turbulence, the k– $\varepsilon$  (RNG) turbulence model was used. Readers are directed to Gorman et al. (2021) and Abraham et al. (2021) for a review of computational fluid dynamic models, turbulence approaches, and the

development of computational fluid dynamics. For solving free surface flow equation, the void of fluid (VOF) method was used (Hirt and Nichols 1981). To discretize the pressure expression, the pressure implicit with splitting of operator (PISO) method and the second-order upward (SOU) method were used to discretize the momentum expression. Numerical simulation of a flow passing over a broad-crested weir in an open channel is a two-phase and turbulent flow. The transfer ratio of the fluid fraction is expressed by Eq. 10.

$$\frac{\partial F}{\partial t} + \frac{\partial \overline{U_i}F}{\partial X_i} = 0 \tag{10}$$

This method is predicated on the fact that two or more fluids do not combine. So, the coordinates and values of each cell represent one of the phases, and the value of the relative volumetric fraction (F) varies from 0 to 1 depending on the concentration of a particular fluid species in the cell. If the cell is full of air, the value of the volume ratio is zero (F=0). On the other hand, if it is completely full of water, F=1. If the cell has both fluids contained within it, then 0 < F < 1. For such a cell, it contains a free surface within it (Ansys Fluent 2015).

## 2.4 Meshing and Boundary Conditions

In a numerical simulation, the computational mesh can affect the model results. In this section, the effect of mesh on modeling results is investigated. To create the mesh, Gambit software was used. The two-dimensional geometry of the model was designed, and then the solution domain was discretized with square-shaped elements.

A mesh-independence test was performed, and the appropriate number of elements was selected. It was found that with an increase in the number of elements from 314 to 20,526, the difference between laboratory and numerical results decreased, as expected. When the number of elements exceeded approximately 16,000, the difference between the laboratory and numerical results no longer changed. Therefore, in this simulation, the appropriate number of elements was 15,860, and the number of nodes was 16,157. Table 2 shows the influence of element number on the jet trajectory for a constant hydraulic and geometric profile.

In the Table 2, N is the number of elements,  $X_{\text{max-S}}$  is the maximum range of the free-falling jets that obtained from simulation, and  $X_{\text{max-E}}$  is the maximum range of the free-falling jet that obtained from experiments. According to Table 2, when the number of elements exceeded 15,860, the difference between the laboratory and numerical results no longer changed. Therefore, in this simulation, the appropriate number of elements was 15,860.

The issue of free-falling jets is related to the drag force or the air resistance force against the movement of the



Table 2 Meshing independent test in the present study

$X_{\text{max}-S}(\mathbf{m})$	$X_{\max-E}(\mathbf{m})$	$X_{\max-S} - X_{\max-E}$
1.157	0.483	0.673
1.148	0.483	0.665235
1.129	0.483	0.645
0.978	0.483	0.494
0.944	0.483	0.461
0.792	0.483	0.309
0.791	0.483	0.308
0.791	0.483	0.308
	1.157 1.148 1.129 0.978 0.944 0.792 0.791	1.157     0.483       1.148     0.483       1.129     0.483       0.978     0.483       0.944     0.483       0.792     0.483       0.791     0.483

falling jet. Numerical simulation of a falling jet in an open channel is a two-phase flow. According to Table 2, it can be seen that the difference in the range of the freefalling jets is still significant between simulations and experiments even by applying the relatively finer mesh by 15,860 elements. The reason for this difference can be due to the lack of air resistance force in this simulation. In Table 2, air resistance has not affected the trajectory for free jets in the calculations. In the simulation of resistance force, the object must be placed against the moving flow or the moving object in the still fluid. In the Fluent software, to apply and calculate the resistance force on the object, that part of the object must be introduced to the software from the beginning. In falling jets simulation, the water jet is formed by the software after solving the model. Before solving the model, it is not possible to introduce this part to apply air resistance. For this reason, the effect of air resistance on the trajectory of the falling jet has not been applied in the Fluent software.

Another important issue in numerical simulation is the proper definition of boundary conditions (BCs). The boundary condition at the inlet is an applied pressure value. At the outlet flow location, a zero pressure is applied. At the downstream side of the rectangular broad-crested weir, a water pressure flow limit condition was used. In addition, the BCs at the channel invert and rectangular broad-crested weir inner surface were wall boundary conditions with a roughness of 0.0001 mm. At the channel top, the condition was a zero outlet pressure.

At the upper boundary of the channel, both zero pressure conditions and symmetry conditions were used, and there was no difference in the results. The depth, velocity, hydraulic radius, and upstream turbulence intensity are entered into the software, and the openness of the upstream canal is determined. The computational mesh and the boundary conditions are shown in Fig. 4. Time step integration was carried out using a time step of 0.001 s and continued until it reached steady conditions.

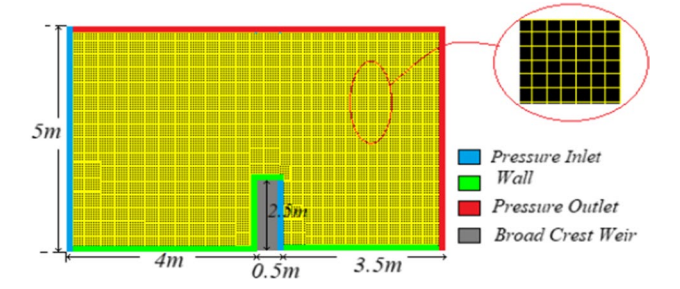


Fig. 4 Computational mesh and boundary conditions

#### 3 Results and Discussion

# 3.1 Proposed Equation for Trajectory of Free-Falling Jet

One hundred experiments were performed with different discharges and widths of different sections. In total, 1600 data points (x and y locations) were extracted from the trajectory of the jet. Figure 5 shows an example of the trajectory of free-falling jet. In Fig. 5, x and y coordinates were normalized with  $h_v$  in which  $h_v$  refers to velocity head and is defined by Eq. 11. In Eq. 11,  $V_0$  is the initial free-falling jet velocity (m/s) and g is the acceleration due to gravity (m/s<sup>2</sup>).

$$h_{v} = \frac{V_0^2}{2g} \tag{11}$$

It can be seen that the trajectory length calculated using Eq. 3 is greater than its actual value because air resistance is ignored. In other words, the actual value of the projectile range is shorter than the value obtained from Eq. 3 due to air resistance. By analyzing the laboratory results and comparing it with the results of the projectile equation, it was found that the trajectory of the falling jet extracted

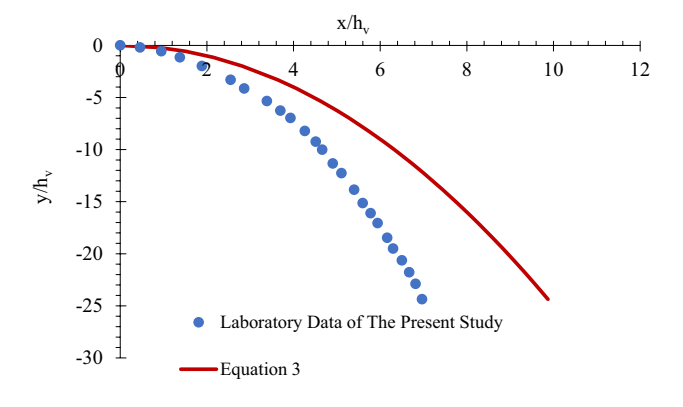


Fig. 5 Trajectory of a free-falling jet (laboratory measurements and projectile equation)



from the equations, compared to its true value (laboratory data), has an average error of about 21%.

When the jet begins horizontally, the governing equation for the projectile is Eq. 2. By simplifying Eq. 2, the trajectory of the jet plane at different altitudes is obtained from the following relation:

$$x = 2\sqrt{(-y)h_y} \tag{12}$$

This equation describes the motion of a projectile that is not affected by air resistance. To incorporate the effect of air resistance on the range of the falling jet, Eq. 12 is modified to be:

$$x = 2\sqrt{(-y)h_y} - \xi \tag{13}$$

In Eq. 13,  $\xi$  modifies the trajectory of the free jet. Laboratory data were used to derive the equation to correct the trajectory of the jet plane. Approximately, 75% of the data were used for training (1200 data), and 25% of the data were reserved for testing (400 data). In order to achieve an equation that can correct the trajectory of the jet fall with reduced error, various equation forms were examined with Eq. 14, and the selected modified form is as follows:

$$\xi = -0.092h_{v} + 0.041y \tag{14}$$

In Eq. 14, y is the fall height of the free-fall jet and  $h_v$  is the velocity head (m) defined by Eq. 11. Given the constant coefficients of Eq. 14, it is observed that the effect of the fall height is less than the approaching velocity (by a factor of 2). At the same time, these two factors work in opposite directions. By combining Eqs. (13) and (14), the trajectory of the jet plane is obtained as Eq. 15.

$$x = 2\sqrt{(-y)h_v} - (0.092h_v - 0.041y) \tag{15}$$

Equation 15 is a relation for predicting the trajectory of the jet plane (range of the falling jet from any altitude). In fact, Eq. 15 is the transform of Eq. 2 with a modification term ( $\xi$ ) to account for air resistance. In addition, to Eq. 15, different relationships were fitted to predict the trajectory of the free-falling jet, and finally Eq. 16 is presented to calculate the position of the jet.

$$\frac{x}{D} = -0.1835 \frac{y}{D} - 0.00072 \left(\frac{y}{D}\right)^2 - 0.04 \frac{P}{D} - 0.000077 \left(\frac{P}{D}\right)^2 
+ 5.833 \frac{H_{\text{overtop}}}{D} - 0.573 \left(\frac{H_{\text{overtop}}}{D}\right)^2 
- 0.00016 \frac{y \times P \times H_{\text{overtop}}}{D^3}$$
(16)

In Eq. 16, x and y are the coordinates of the lower edge of the jet, D is the width of the outlet of the free jet, P is the height of the drop from the ground, and  $H_{\text{overtop}}$  is the head

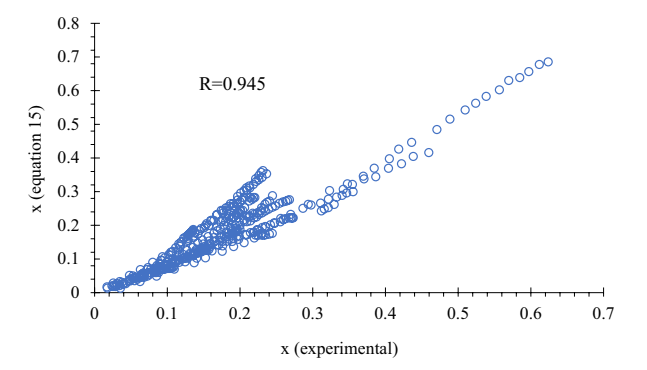
passing through the structure. To investigate the accuracy of Eqs. (15) and 16), two scatter plots are provided for experimental data (Fig. 6).

According to Fig. 6, it can be seen that most of the data are located near the semicircle of the first region, which indicates the accuracy of the relationships at calculating the trajectory of the free jet. Also, the high value of the correlation coefficient (*R*) of these graphs shows the high accuracy of these graphs in predicting the trajectory of the free jet.

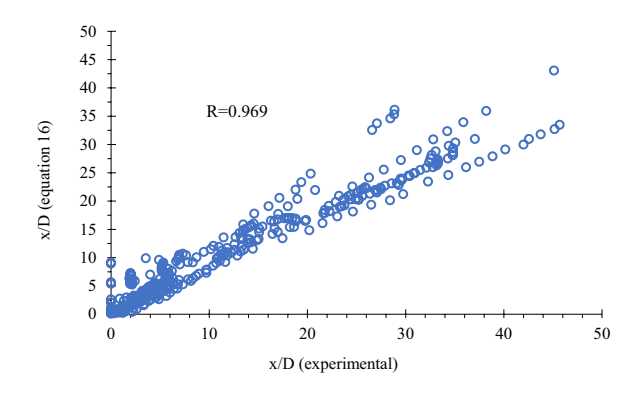
# 3.2 Results of Numerical Simulations

Figure 7 shows the trajectory of the free-falling jet from the start until a steady state is achieved. In the figure, the spillway height is 2 m, the spillway crest length is 0.5 m, the spillway head height is 31 cm, and the upstream flow velocity of the canal is 0.15 m/s. In the figure, red colors correspond to water-filled regions, whereas blue cells are air-filled. Mixed cells (including air and water) are indicated by other contour colors.

Figure 7 shows the water surface profile in which the two phases (air and water) are separate. It can be seen that after



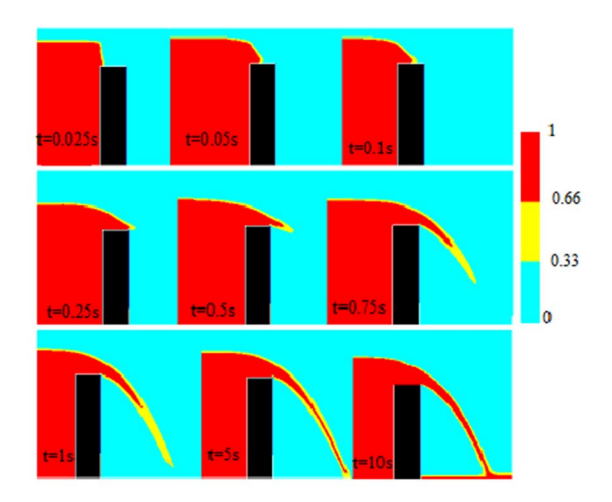
(a) Scatter plot of Eq. (15) data using the test data (25% of data)



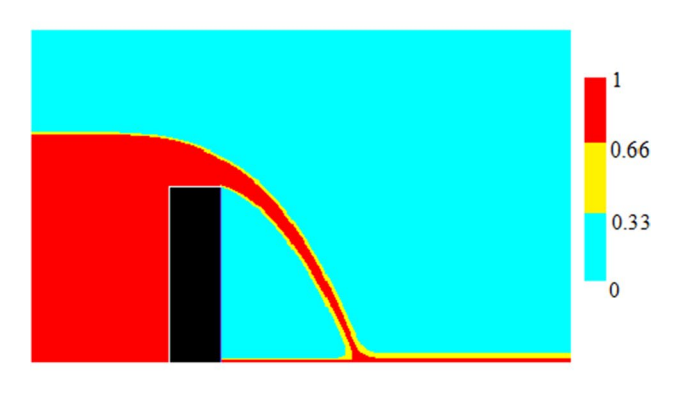
(b) Scatter plot of Eq. (16) data using test data (25% of data)

**Fig. 6** Scatter plots for test data. **a** Scatter plot of Eq. (15) data using the test data (25% of data) **b** Scatter plot of Eq. 16 data using test data (25% of data)





(a): Trajectory of free falling jet in different time steps



(b): Details of trajectory including air-water phase ratios

Fig. 7 Free-fall jet trajectory in numerical simulation

about 0.25 s, the jet reaches the end of the broad-crest weir, and after about one second, the falling jet hits the spillway toe. After 10 s, the jet reaches a steady-state condition. Also, according to Fig. 7, some of the free-falling jets returns toward the spillway face (the black rectangle in Fig. 7), and some moves downstream of the canal.

In the numerical simulation of rectangular broad-crested weir, if the wall condition is selected for the downstream side of the rectangular broad-crested weir, after the model is solved by the Ansys Fluent software, the falling jet sticks to the body of the structure. In this situation, the falling flow loses its projectile shape. In numerical simulations of the present study, at the downstream side of the rectangular broad-crested weir, a water pressure flow condition to aerate the weir and prevent the water jet from sticking to the body of the weir was used. According to Fig. 3, in the laboratory work, aeration is not required for rectangular broad-crested weir, and air is between the falling jet and weir. Figure 8

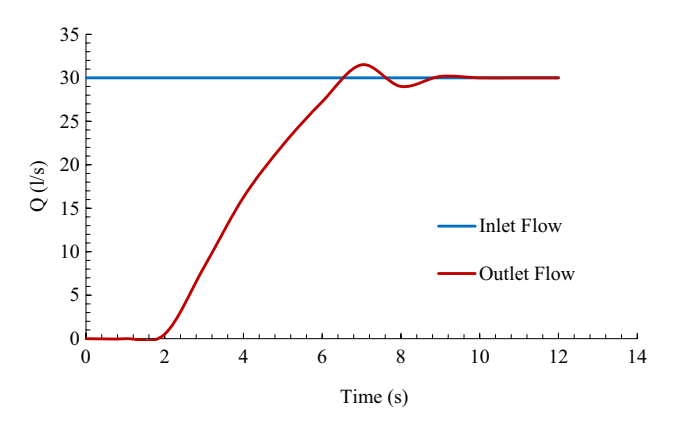


Fig. 8 Inlet and outlet flow hydrograph to the channel

shows the inlet and outlet hydrographs in the simulated channel.

According to Fig. 8, the steady-state flow is 30 l/s. It can be seen that initially, no flow leaves the system; however, the outflow flow slowly increases until it reaches equilibrium with the inlet flow, as required for steady state. In other words, after 10 s, the amount of discharge that enters the channel is equal to the amount of discharge that leaves the channel, a requirement for a steady-state condition. Figure 8 shows that for short instances, the exit flow exceeds the inlet discharge. When the free-falling jet hits the ground, some of the discharge returns to the structure. The reason for this increase in flow is the return of water from the toe of the dam to the outlet. In other words, in the hydrograph of Fig. 8 and in the 7th second, the outlet flow rate from the model is higher than the inlet. At the beginning, when the freefalling jet hits the ground, some of the discharge returns to the structure (according to Fig. 7b). When this flow hits the rectangular broad-crested weir, it moves downstream again. The reason for this increase in flow in 7th second is the return of water from the toe of the weir to the outlet.

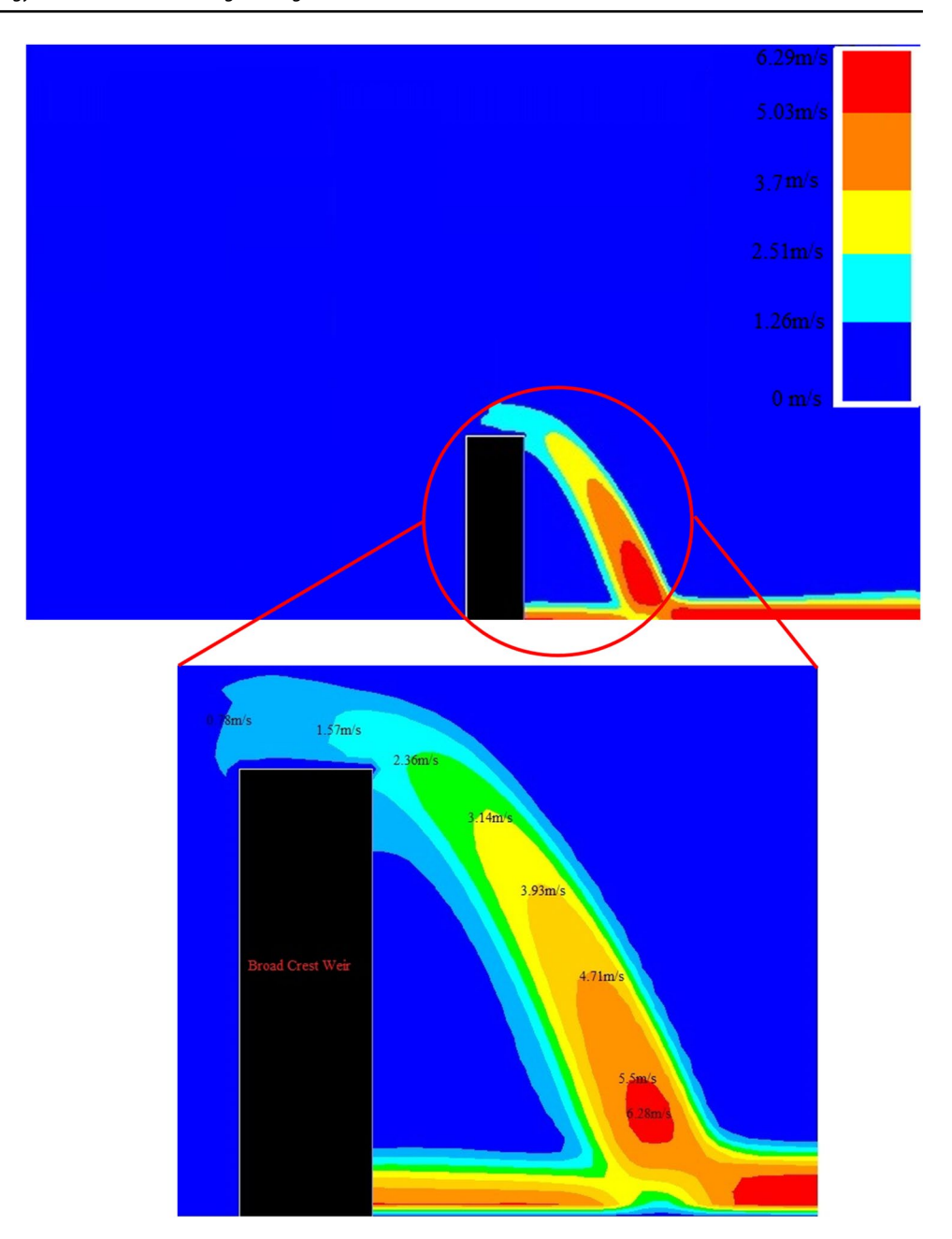
Figure 9 shows the flow velocity contours after numerical simulation and after reaching a steady state (after 10 s) in the above flow conditions.

As shown in Fig. 9, the velocity is increased over the spillway and the flow velocity at the end of the spillway crest is 2.51 m/s and after the flow separates from the spillway and forms a free-falling jet and the jet collides with the bottom of the canal. The velocity at the end of the canal and in a position above the point of impact to the ground reaches its maximum value of 6.2 m/s. It can be noted that upstream of the broad-crested weir has been simulated as a dam reservoir, and thus, the approach velocity behind of weir is near zero as indicated in legend of Fig. 9.

In fluid mechanics, pressure is the normal force applied to a surface. Static pressure (sometimes called hydrostatic pressure) is the pressure exerted by a fluid at rest. This fluid



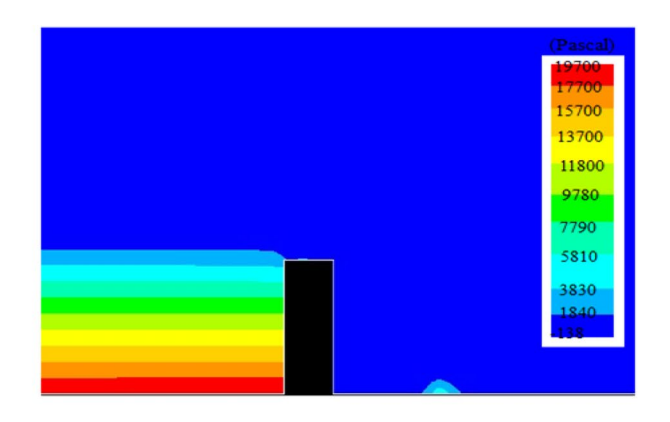
Fig. 9 Velocity contours

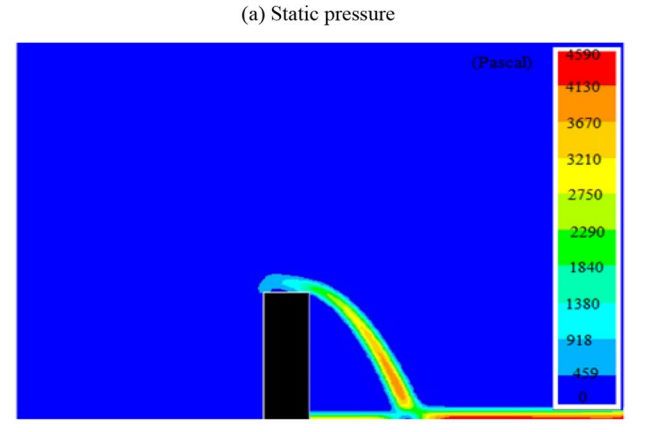


can be liquid or gas. Since the fluid does not move, the static pressure is the result of the weight of the fluid or the gravitational force on the fluid particles. Dynamic pressure is a pressure associated with the movement of the fluid. In other word, dynamic pressure is dependent on fluid velocity and Bernoulli's principle and is one of the terms of Bernoulli's equation. In fluid dynamics, total pressure is equal to the sum of two dynamic and static pressures of a free flow. It should be noted that after simulating the flow of a free-falling jet in the Ansys Fluent software, by selecting each of these pressures, the software presents their values to the user. Figures 10a–c shows the static, dynamic, and total pressures (in Pascal or N/m²), respectively.

According to Fig. 10a, it is observed that downstream of the dam, the static pressure at the point of impact of the jet is higher than other points downstream of the dam. Figure 10b shows that the dynamic pressure increases due to the increase in velocity downstream of the channel. The total pressure, which is the sum of dynamic and static pressure, is shown in Fig. 10c. It can be seen that the total pressure upstream is mainly due to static pressure and downstream caused by both static and dynamic pressures.







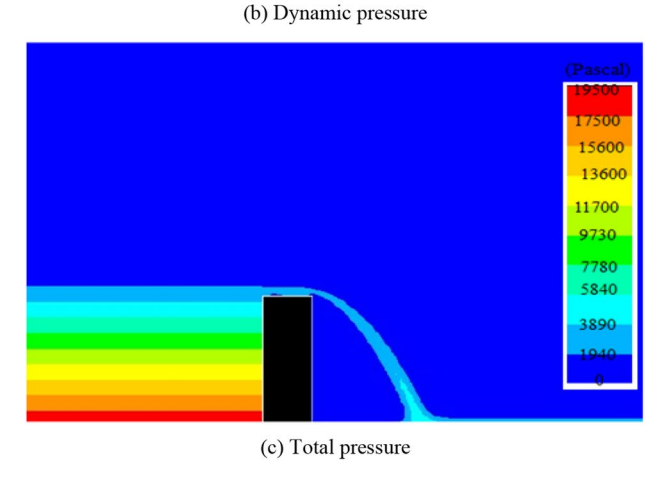


Fig. 10 Pressure change contours (numerical values in Pascals)

# 3.3 Comparison of the Trajectory Equations

In this section, the free-fall jet trajectories are examined and compared using the laboratory results and numerical simulations. In addition, the comparison includes results from other researchers (Fig. 11).

Figure 11 shows the trajectory of a free-falling jet under the conditions specified in the diagram using various relationships and laboratory data as well as data extracted from numerical simulations. In addition, an ogee spillway with the same water height on the spillway was designed for this comparison. Valuable studies have been performed by USBR (1987) to design this type of dam spillway. Based on data from this organization, the Water Research Institute at USACE has provided several shapes to determine the downstream curve in ogee spillways. If a general ogee spillway is considered, the curve in front of the crest of this type of spillway (the downstream face) follows Eq. 16 (Kabiri Samani and Bagheri 2014). In the present study, Eq. 16 is used to draw the curve in downstream of the spillway crest including vertical upstream face.

$$\left(\frac{x}{H}\right)^{1.85} = 2 \times \left(\frac{y}{H}\right) \tag{17}$$

In Eq. 17, x and y are the coordinates of the spillway invert, the origin of which is at the highest point of the crest, and H is the design head. In laboratory conditions, various factors affect the trajectory of the free-falling jet, one of the most important of which is air resistance. The air resistance causes a force to be applied to it against the direction of motion of the impinging jet, and the trajectory traveled by the impinging jet is less than the value calculated using different equations. According to Fig. 11, it can be seen that if the laboratory data are considered as a basis, the minimal error corresponds to the equations extracted in the present study (Eq. 15, 16), and the highest error is related to Eq. 5.

In addition, according to Fig. 11, the trajectory of the free-falling jet extracted from Eq. 3 and the equation presented by the US Army Engineers (Eq. 7) corresponds very well with the curve of the downstream crest of the ogee spillway and the simulated trajectory in Ansys Fluent software, and these three trajectories are close. The trajectory calculated using Eq. 5 with k = 0.9, and also assuming  $d + h_v = H_{\text{ovetop}}$  has a large error compared to laboratory data.

Equation 5 may seem simple at first, because it is obtained by a change in Eq. 3. In the case of flow passing through a dam, if the losses are ignored,  $d + h_v$  is approximately equal to the head passing through the dam. Comparing Eqs. 3 and 5, which are obtained directly from the projectile motion equation, it can be seen that these equations are not equal even when K = 1. When K = 1, Eqs. 3 and 5 are dimensionally similar but are not numerically equal. Equation 5 will be true if the entire head passing through the dam ( $H_{overtop}$ ) is converted to the velocity head ( $h_v$ ). As a first approximation, for flow through the dam, the depth and velocity must be critical. Further confusion arises because most citations that use Eq. 5 do not clearly define the terms d and  $h_v$  in the text. If Eq. 5 is used, the falling jet profile becomes less steep and gentler. (The



**Fig. 11** Trajectory comparison, present equations, present experiments, and prior predictive equations

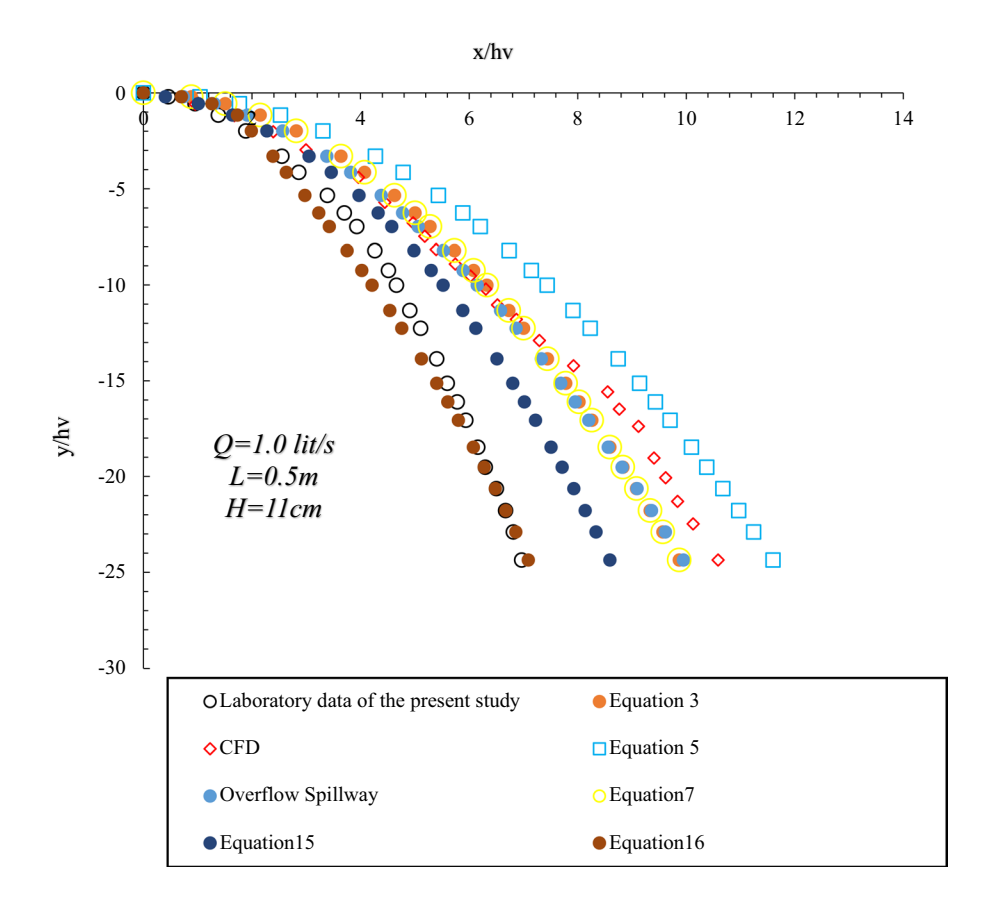


**Table 3** Trajectory error comparison, relative to the laboratory data (for total data)

Data and equations	RMSE	Relative error (%)	
Laboratory data of the present study	0	0	
Equation 16	0.21	3.02	
Equation 15	0.95	9.14	
Overflow spillway (Eq. 17)	1.67	18.05	
Equation 3	1.88	19.35	
Equation 7	1.88	19.34	
CFD	2.1	25.5	
Equation 5	2.9	38.95	

distance between the jet colliding point in the plunging pool and the dam body increases.)

None of the publications presenting this equation has a specific reason for including the term depth. In general, the accuracy of the equations presented in the present study are superior to other equations. Also, the trajectory extracted from Eqs. 3 and 7, as well as the ogee spillway curve, has more acceptable results than numerical simulations and other equations.

The graph in Fig. 11 is randomly selected from about 100 experiments series. Table 3 presents the statistical characteristics for total data.

According to Table 3, it can be seen that if the laboratory data are considered as a basis, the minimal error corresponds to the equations extracted in the present study (Eqs. 15, 16), and the highest error is related to Eq. 5.

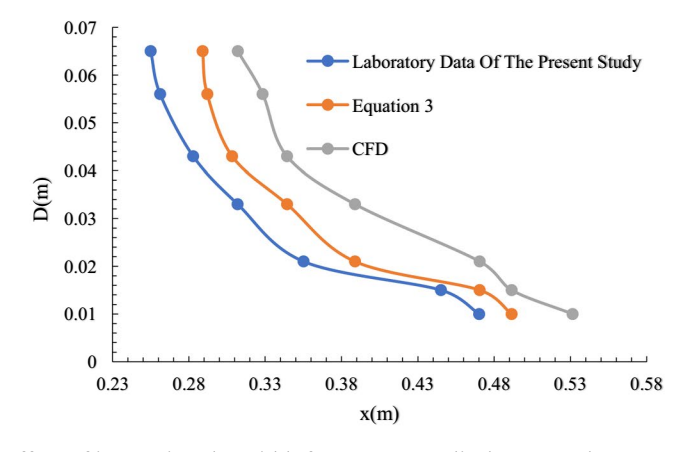
# 3.4 Effect of Head and Cross Section Width on Falling Jet

By increasing the flow velocity and according to the projectile equation (Eq. 1), the distance of the falling jet impact with the river bed increases. In addition, for a constant discharge, the flow velocity decreases and the falling jet range decreases with increasing cross-sectional width. Figure 12a, b shows the trend diagram with increasing width for a fixed discharge and increasing the discharge for a fixed width on the range of a falling jet at a height of 2 m from the edge of a rectangular broad-crest weir.

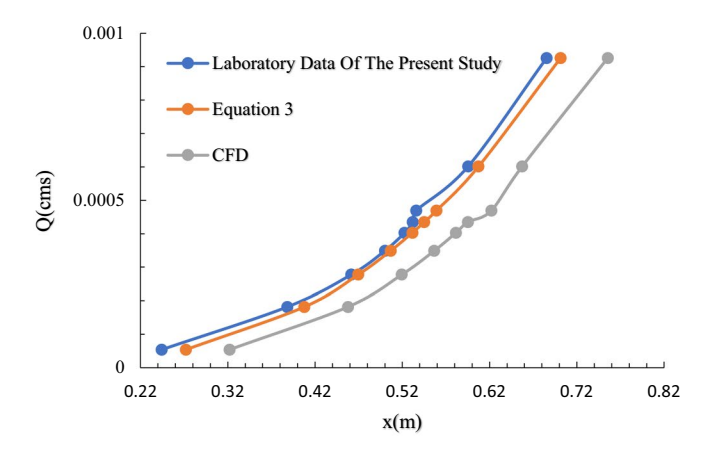
According to Fig. 12a, b, it can be seen that for all three cases studied (laboratory data, data obtained from numerical simulation and projectile equation), by increasing the cross-sectional width of the rectangular broad-crest weir, the lesser the range of jet. With increasing discharge through the spillway, the range of the jet increases. In other



**Fig. 12** Effect of width and discharge on the domain of a free-falling jet



(a) The effect of increasing the width for a constant discharge on the range of the jet plane



(b) The effect of increasing the discharge for a constant width on the range of the jet plane

words, for a constant discharge, with increasing width, the place where the jet falls to the ground surface is closer to the toe of the dam, and for a constant width, with increasing discharge, the place where the jet falls to the ground surface is farther from the toe of the dam.

# **4 Conclusions**

Few studies have been done on the trajectory of falling jets over storage dams. In the present study, the trajectory of falling jets was investigated experimentally and numerically. The height of the falling jet over the dam spillway in the laboratory model was 2.5 m. The results show that the trajectory of falling jets is affected by air resistance, and the range of falling jets in laboratory work is less than the values calculated by various equations that omit air resistance.

Also, the effect of the passing head on the dam and the width of the flow passage section on the range of the free-falling jet was investigated, and the results showed that decreasing the width at constant discharge and increasing the passing head over the dam at constant width increased the falling jet range. Also, Eq. 5, which has been used in various sources, should not be used to determine the direction of a jet downfall. Also, Eqs. 15 and 16 (presented in the present study, respectively, with R = 0.945 and RMSE = 0.95 for Eq. 15 and R = 0.969 and RMSE = 0.21 for Eq. 16) incorporate most parameters involved in free-falling jet and can be used to predict the trajectory satisfactorily.

The simulation results also showed that the velocity and pressure of the flow at the point of impact of the jet to the toe of the dam have its maximum value that should be considered in design.

**Acknowledgements** This research did not receive any specific grant from funding agencies in the public, commercial, or not-for-profit sectors.



**Data Availability** Some or all data, models, or code that support the findings of this study are available from the corresponding author upon reasonable request.

#### **Declarations**

**Conflict of interest** The authors declare no competing interests.

**Ethical Approval** This article does not contain any studies with human participants or animals performed by any of the authors.

# References

- Abraham JP, Bhattacharya S, Cheng L, Gorman JM (2021) A brief history of and introduction to computational fluid dynamics. In: Bhattacharya S (ed) Computational fluid dynamics. IntechOpen. https://doi.org/10.5772/intechopen.97235
- Annandale GW (2006) Scour technology: mechanics and engineering practice. McGraw-Hill, New York, pp 146–151
- Bureau of Reclamation (1977) Design of arch dams. United States Department of the Interior, United States Government Printing Office, Denver, pp 312–313
- Davis AC, Jacob RP, Ellett BGS (1999) Estimating trajectory of free overfall nappe. J Hydraul Eng 125(1):79–82
- Delleur JW, Dooge JCI, Gent KW (1956) Influence of slope and roughness on the free overfall. In: Proceedings of American Society of Civil Engineers, vol 82, no HY4, p 1038. 1038-30-1038-35
- Ansys Fluent (2015) Tutorial guide
- Gorman JM, Bhattacharya S, Abraham JP, Cheng L (2021) Turbulence models commonly used in CFD. In: Bhattacharya S (ed) Computational fluid dynamics. IntechOpen. https://doi.org/10.5772/ intechopen.99784
- Henderson FM (1966) Open channel flow. MacMillan, New York, pp 191–197
- Hirt W, Nichols BD (1981) Volume of fluid (VOF) method for the dynamics of free boundaries. J Comput Phys 39:201–225
- Samani K, Bagheri ARS (2014) Design of channels and water conveyance structures. Arkan Danesh Publications, pp 264–269. (In Persian)
- Malekzadeh F, Salmasi F, Abraham J, Arvanaghi H (2022) Numerical investigation of the effect of geometric parameters on discharge coefficients for broad-crested weirs with sloped upstream and downstream faces. Appl Water Sci 12:110. https://doi.org/10. 1007/s13201-022-01631-5
- Nourani B, Arvanaghi H, Salmasi F (2021) Effects of different configurations of sloping crests and upstream and downstream ramps

- on the discharge coefficient for broad-crested weirs. J Hydrol 603(Part B):126940. https://doi.org/10.1016/j.jhydrol.2021. 126940
- Rouse H (1936) Discharge characteristics of the free over fall. Civ Eng 6:257
- Rouse H (1943) Discussion of energy loss at the base of a free overfall. Trans Am Soc Civ Eng 108:1383–1387
- Salemnia A, Fathi Moghadam M (2019) Investigation of break up length of free water jet. Iran J Irrig Drain 2(13):309–318 (In **Persian**)
- Salmanzadeh S, Ahadiyan J (2016) Distribution limit of jet flow in the same and dissimilar phases of ambient fluid. Irrig Sci Eng 1(36):93–107 (**In Persian**)
- Salmasi F, Abraham J (2022) Multivariate nonlinear regression for predicting free falling-jet scouring: an experimental study. Iran J Sci Technol Trans Civ Eng. https://doi.org/10.1007/s40996-022-00817-w
- Salmasi F, Samadi A (2018) Experimental and numerical simulation of flow over stepped spillways. Appl Water Sci 8(229):1–11. https://doi.org/10.1007/s13201-018-0877-5
- Salmasi F, Nourani B, Arvanaghi H, Rezaei F (2022) Undular Flow Conditions and Discharge Coefficient in Rectangular Broad-Crested Weirs. Amirkabir J Civ Eng 54(1):8–8. https://doi.org/ 10.22060/ceej.2021.18314.6830. (In Persian)
- USACE (1964) High overflow dams, energy dissipators, flip bucket throw distance. U.S. Army Corps of Engineers, Hydraulic design criteria, sheet 112-8, Coastal and Hydraulics Laboratory, Engineer Research and Development Center, Waterways Experiment Station, Vicksburg, Miss
- USBR (1960) Design of small dams, US Bureau of Reclamation 1st edn. United States Department of the Interior, United States Government Printing Office, Denver, pp 282291.
- Design of gravity dams, US Bureau of Reclamation. United States Department of the Interior, United States Government Printing Office, Denver, pp 198–199
- Wahl TL, Frizell KH, Cohen EA (2008) Computing the trajectory of free jets. J Hydraul Eng 134(2):256–260
- Yıldız A, Yarbaşı GE, Yarar A, Ihsan Marti A (2020) Modeling of broad crested weirs by using dynamic similarity and CFD. Rom J Ecol Environ Chem 2(2):2668. https://doi.org/10.21698/rjeec. 2020.212

Springer Nature or its licensor (e.g. a society or other partner) holds exclusive rights to this article under a publishing agreement with the author(s) or other rightsholder(s); author self-archiving of the accepted manuscript version of this article is solely governed by the terms of such publishing agreement and applicable law.

